The Journal of Immunology

Regulation of Cell Adhesion by Affinity and Conformational Unbending of $\alpha_4\beta_1$ Integrin

Alexandre Chigaev, Anna Waller, Gordon J. Zwartz, Tione Buranda and Larry A. Sklar

J Immunol 2007; 178:6828-6839; ;
doi: 10.4049/jimmunol.178.11.6828
http://www.jimmunol.org/content/178/11/6828

The Journal of Immunology is published twice each month by
The American Association of Immunologists, Inc.,
1451 Rockville Pike, Suite 650, Rockville, MD 20852

Print ISSN: 0022-1767 Online ISSN: 1550-6606.

Regulation of Cell Adhesion by Affinity and Conformational Unbending of $\alpha_4\beta_1$ Integrin[1]

Alexandre Chigaev,[2] Anna Waller, Gordon J. Zwartz, Tione Buranda, and Larry A. Sklar

Rapid activation of integrins in response to chemokine-induced signaling serves as a basis for leukocyte arrest on inflamed endothelium. Current models of integrin activation include increased affinity for ligand, molecular extension, and others. In this study, using real-time fluorescence resonance energy transfer to assess $\alpha_4\beta_1$ integrin conformational unbending and fluorescent ligand binding to assess affinity, we report at least four receptor states with independent regulation of affinity and unbending. Moreover, kinetic analysis of chemokine-induced integrin conformational unbending and ligand-binding affinity revealed conditions under which the affinity change was transient whereas the unbending was sustained. In a VLA-4/VCAM-1-specific myeloid cell adhesion model system, changes in the affinity of the VLA-4-binding pocket were reflected in rapid cell aggregation and disaggregation. However, the initial rate of cell aggregation increased 9-fold upon activation, of which only 2.5-fold was attributable to the increased affinity of the binding pocket. These data show that independent regulation of affinity and conformational unbending represents a novel and fundamental mechanism for regulation of integrin-dependent adhesion in which the increased affinity appears to account primarily for the increasing lifetime of the $\alpha_4\beta_1$ integrin/VCAM-1 bond, whereas the unbending accounts for the increased capture efficiency. *The Journal of Immunology,* **2007, 178: 6828–6839.**

Capture, rolling, and firm adhesion on endothelium are key steps that regulate targeting and extravasation of leukocytes to the sites of inflammation. Integrins, selectins, and their counterstructures determine cell adhesive properties in these processes (1). Rapid changes in integrin-dependent cell avidity in response to activation of G protein-coupled receptors (GPCRs)[3] ("inside-out" activation) have been attributed to subsecond clustering of integrins (2), as well as to a large conformational rearrangement of the molecule itself, which is believed to be accompanied by a change in affinity for ligand (3). The x-ray structure of the $\alpha_v\beta_3$ integrin ectodomain revealed a bent conformation (4) that has been confirmed by alternate methods (5–8). Electron microscopy images showed the bent and extended forms of the recombinant integrin in solution (8).

A "switchblade-like" model of integrin activation was proposed from the analysis of the integrin EGF domain and exposure of integrin activation epitopes. This model implies a large conformational change in which the head of the integrin molecule moves away from the plasma membrane while the affinity for the ligand changes (9, 10). The existence of the extended conformation in which the ligand-binding pocket is exposed, and therefore facilitates the encounter between integrin and endothelial adhesion molecule, supports the possibility of a mechanism to regulate tethering and rolling on low-affinity extended integrins (11). It is well documented that some of the integrins can support tethering and rolling of leukocytes in shear flow (12, 13). However, the physiological ligand is able to bind bent integrin in solution in a Mn^{2+}-dependent manner, raising the possibility that a small localized conformational change is enough to up-regulate the affinity of the binding pocket (5). Moreover, analysis of Ab competition patterns for resting or agonist-activated $\alpha_{IIb}\beta_3$ on platelets suggested a "piston and rotation" movement of the transmembrane segments along the membrane, arguing against association of a switchblade mechanism with integrin activation (14). It is also possible that variable extended conformations with intermediate and high affinity to ligand are present on cell surfaces (15). Thus, regulation of the affinity state of the integrin-binding pocket and the conformational unbending of the molecules represents a fundamental issue that is important for understanding the molecular mechanisms responsible for tethering, rolling, and arrest of leukocytes on inflamed endothelium.

We sought to address this issue using a novel set of tools that allows us to monitor affinity state, as well as conformational unbending of the $\alpha_4\beta_1$-integrin (VLA-4 and CD49d/CD29) on living cells. Changes in VLA-4 affinity can be detected in real-time and on a physiologically relevant time frame using a ligand-mimicking LDV-containing fluorescent small molecule (4-((*N*′-2-methylphenyl)ureido)-phenylacetyl-L-leucyl-L-aspartyl-L-valyl-L-prolyl-L-alanyl-L-alanyl-L-lysine-FITC (LDV-FITC)) (16). Previous competition studies showed that dissociation rates for the natural VLA-4 ligand, VCAM-1, and the LDV-FITC probe varied in parallel (17). For several different receptors, the physiologically activated state of the integrin, determined by inside-out signaling, has similar affinity in several cell types (7, 16, 18, 19). Using the same VLA-4-specific probe, we developed a fluorescence resonance energy transfer (FRET) assay to investigate the dynamic structural transformation of VLA-4 in response to cell stimulation (6). Change in the FRET signal was

Department of Pathology and Cancer Center, University of New Mexico Health Sciences Center, Albuquerque, NM 87131

Received for publication September 7, 2006. Accepted for publication March 15, 2007.

The costs of publication of this article were defrayed in part by the payment of page charges. This article must therefore be hereby marked *advertisement* in accordance with 18 U.S.C. Section 1734 solely to indicate this fact.

[1] This work was supported by National Institutes of Health Grants EB02022 and HL56384 (to L.A.S.), Leukemia and Lymphoma Society Grant 7388-06 (to L.A.S.), and AI60036 (to T.B.).

[2] Address correspondence and reprint requests to Dr. Alexandre Chigaev, Department of Pathology, University of New Mexico HSC, Albuquerque, NM 87131. E-mail address: achigaev@salud.unm.edu or Dr. Larry A. Sklar, Department of Pathology, University of New Mexico HSC, Albuquerque, NM 87131. E-mail address: lsklar@salud.unm.edu

[3] Abbreviations used in this paper: GPCR, G protein-coupled receptor; FPR, formyl peptide receptor; FRET, fluorescence resonance energy transfer; HSA, human serum albumin; MCF, mean channel fluorescence, equivalent of mean fluorescence intensity; PKC, protein kinase C; PLC, phospholipase C, CD106.

interpreted as a change in the distance of closest approach or molecular unbending of ~25–50 Å upon activation (see Fig. 1) (6, 7).

The goal of the current work was to resolve the relationship between VLA-4 affinity changes detected using the LDV-FITC probe-binding assay and molecular unbending using the FRET assay and to explore a functional role of these two features of the molecule in the regulation of VLA-4-dependent cellular adhesion. Our results define distinct signaling mechanisms that independently regulate the affinity of the ligand-binding pocket, as well as the molecular unbending of VLA-4 from inside the cell. Modulation of the affinity of the binding pocket resulted in the rapid changes in the adhesion avidity of cells in suspension as detected in real time. The overall number of aggregates at steady state was regulated by the ligand dissociation rate and the lifetime of the aggregate. However, different states of molecular unbending at similar affinity state of the binding pocket were reflected in different initial rates of cell aggregation: the unbent state exhibited a 3- to 4-fold faster initial aggregation rate. We discuss the roles for the independent regulation of integrin affinity and conformational unbending, a novel and fundamental mechanism by which leukocyte capture, rolling, and arrest are regulated in response to chemokine-induced inside-out signaling.

Materials and Methods

Materials

The VLA-4-specific ligand (6, 16, 17) 4-((N′-2-methylphenyl)ureido)-phenylacetyl-L-leucyl-L-aspartyl-L-valyl-L-prolyl-L-alanyl-L-alanyl-L-lysine (LDV containing small molecule) and its FITC-conjugated analog (LDV-FITC) were synthesized at Commonwealth Biotechnologies. Octadecyl rhodamine B chloride (R18), fluo-4AM, hydroethidine, and CFSE were from Molecular Probes. PE-conjugated anti-human CD106 (VCAM-1) was purchased from BD Pharmingen. FITC-conjugated mAb 44H6, against human CD49d (α_4 integrin subunit), was purchased from Serotec. mAb HP2/1, against human CD49d, was purchased from Immunotech. All restriction enzymes were purchased from New England Biolabs. All other reagents were from Sigma-Aldrich. Stock solutions of probes were prepared in DMSO, except for A23187 prepared in ethanol, at concentrations ~1000-fold higher than the final concentration. Usually, 1 μl of stock solution was added to 1 ml of cell suspension, yielding a final DMSO concentration of 0.1%. Control samples were treated with equal amount of pure DMSO or ethanol.

Cell lines and transfectant construct

The mouse melanoma cell line B78H1 and the human monoblastoid cell line U937 were purchased from American Type Culture Collection. Site-directed mutants of the formyl peptide receptor (FPR; nondesensitizing mutant of FPR ΔST) in U937 cells were prepared as previously described (20) and were a gift from Dr. E. Prossnitz (University of New Mexico, Albuquerque, NM). For transfection of B78H1 cells, full-length human VCAM-1 cDNA was a gift from Dr. R. Lobb of Biogen Idec (Cambridge, MA). The original construct (21) was subcloned into the pTRACER vector (Invitrogen Life Technologies). Transfection into B78H1 was done using the LipofectAMINE Reagent (Invitrogen Life Technologies). High receptor-expressing cells were selected using the MoFlo Flow Cytometer (DakoCytomation). Cells were grown at 37°C in a humidified atmosphere of 5% CO_2 and 95% air in RPMI 1640 (supplemented with 2 mM L-glutamine, 100 U/ml penicillin, 100 μg/ml streptomycin, 10 mM HEPES (pH 7.4), and 10% heat-inactivated FBS). Cells were then harvested and resuspended in 1 ml of HEPES buffer (110 mM NaCl, 10 mM KCI, 10 mM glucose, 1 mM $MgCI_2$, and 30 mM HEPES (pH 7.4)) containing 0.1% human serum albumin (HSA) and stored on ice. The buffer was depleted of LPS by affinity chromatography over polymyxin B-Sepharose (Detoxigel; Pierce). Cells were counted using the Coulter Multisizer/Z2 analyzer (Beckman Coulter). For experiments, cells were suspended with the same HEPES buffer at 1×10^6 cells/ml and warmed to 37°C. Alternatively, cell were resuspended in dye-free warm RPMI 1640 or HEPES buffer (37°C) and used immediately. The expression of adhesion molecules was measured with fluorescent mAbs and quantified by comparison with a standard curve generated with Quantum Simply Cellular microspheres (Bangs Laboratories) stained in parallel with the same mAb. This produces an estimate of the total mAb binding sites/cell. Typically, we find 400,000–600,000 VCAM-1 sites per B78H1 cell and 40,000–60,000 VLA-4 sites per U937 cell.

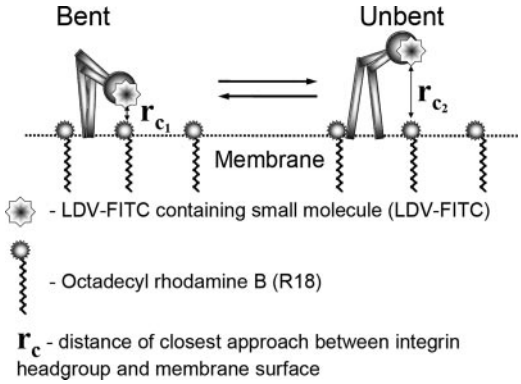

FIGURE 1. Cartoon depicting FRET assay for assessing VLA-4 conformational unbending. Energy transfer between VLA-4 head groups and lipid probes incorporated into the plasma membrane provides a way of studying integrin conformational unbending. The LDV-FITC probe that specifically binds to the head group of VLA-4 is used as a fluorescent donor at a high enough concentration (100 nM) to saturate all low-affinity resting binding sites. A change in VLA-4 affinity would not affect probe binding. Octadecyl rhodamine B (R18), a lipophilic probe, inserts into the membrane as an acceptor. Upon activation, VLA-4 assumes an unbent (upright) conformation. r_{C1} and r_{C2} are the distances of closest approach before and after molecular unbending. Changes in the fluorescence of the donor were measured on live cells in real time at 37°C by flow cytometry (6, 7).

Kinetic analysis of binding and dissociation

Kinetic analysis of the binding and dissociation of the LDV-FITC probe was described previously (16). Briefly, U937 cells (1×10^6 cells/ml) were preincubated in HEPES buffer containing 0.1% HSA at different conditions for 10–20 min at 37°C. Flow cytometric data were acquired for up to 1024 s at 37°C, while the samples were stirred continuously at 300 rpm with a 5 × 2-mm magnetic stir bar (Bel-Art Products). Samples were analyzed for 30–120 s to establish a baseline. The fluorescent ligand was added, and acquisition was re-established, creating a 5- to 10-s gap in the time course. For real-time affinity activation experiments, 4 nM LDV-FITC probe was added after establishing a baseline for unstained cells marked on figures as "autofluorescence." Then, data were acquired for 2–3 min, and *N*-formyl-L-methionyl-L-leucyl-L-phenylalanyl-L-phenylalanine (fMLFF) (100 nM), PMA (0.5 nM–1 μM), A23187 (10–40 μg/ml), U-73122 (20 nM–2 μM), or Mn^{2+} (1 mM) was added. In several experiments, cells were treated sequentially with two or more different compounds. Acquisition was re-established, and data were acquired continuously for up to 1024 s.

The concentration of the LDV-FITC probe used in the experiments (4 nM) was below the K_d for its binding to resting VLA-4 (low-affinity state 1, K_d ~12 nM) and above the K_d for physiologically activated VLA-4 (high-affinity state 2, K_d ~1–2 nM) (16). Therefore, the transition from the low-affinity to the high-affinity receptor state led to increased binding of the probe (from ~25 to ~70–80% of receptor occupancy, as calculated based on the one site-binding equation), which was detected as an increase in the mean channel fluorescence (MCF). For kinetic dissociation measurements, cell samples were preincubated with the fluorescent probe (4–10 nM) and treated with excess unlabeled LDV-containing small molecule (2 μM), and the dissociation of the fluorescent molecule was followed. The resulting data were converted to MCF vs time using FCSQuery software developed by Dr. B. Edwards (University of New Mexico, Albuquerque, NM).

FRET detection of VLA-4 conformational unbending

The FRET assay used the LDV-FITC probe as a donor, which specifically binds to the α_4 integrin head group, and octadecyl rhodamine B (R18) as an acceptor incorporated into the plasma membrane (Fig. 1) and was previously described in detail in Ref. 6. Briefly, U937 cells stably transfected with the nondesensitizing mutant (ΔST) of the FPR (22, 23) were preincubated with 100 nM LDV-FITC probe in HEPES buffer containing 1.5 mM $CaCl_2$, 1 mM $MgCl_2$, and 0.1% HSA at 37°C. Alternatively, 100 nM LDV-FITC probe was added after establishing a baseline for unstained

cells (autofluorescence). Next, samples were analyzed for 1–3 min to establish a baseline for 100 nM LDV-FITC, and then, a saturating amount of octadecyl rhodamine B (R18, 10 μM final) was added to yield maximal quenching of donor fluorescence. One to 3 min after R18 was added, cells were treated with fMLFF (100 nM), PMA (0.5 nM–1 μM), A23187 (10–40 μg/ml), ATP (10 μM), or U-73122 (20 nM–2 μM). In several experiments, cells were treated sequentially with two or more different compounds as in the LDV-FITC probe-binding experiments. Donor intensities (FL1 in MCF units) were measured using a Becton Dickinson FACScan flow cytometer at 37°C. Changes in the donor fluorescence intensity were interpreted as changes in the distance of closest approach between LDV-FITC ligand binding site on VLA-4 and the surface of the plasma membrane (r_c; Fig. 1) (6, 7). As previously reported, based on analysis of steady-state FRET measurements, the distance of the closest approach between LDV-FITC and membrane increased for ~25 Å after fMLFF activation, ~50 Å for Mn^{2+}-activated receptors, and ~75 Å for reducing agent in presence of Mn^{2+}. The uncertainty of the head group placement in the resting state was ~25 Å (6, 7). As the length of fully extended integrin is ~200 Å, the change in the distance of closest approach is far from full molecular extension. Therefore, the term "unbending" is more suitable for the description of integrin conformational change. However, the current interpretation of FRET data depends on whether all integrins respond to the inside-out signaling (as the measurements are averaged) and the exact position of the resting integrin (see *Discussion* for more details).

Cell adhesion assay

The cell suspension adhesion assay has been described previously (17). Briefly, U937/ΔST FPR stably transfected cells were labeled with red fluorescent hydroethidine, and B78H1/VCAM-1 transfectants were stained with green CFSE. Labeled cells were washed, resuspended in HEPES buffer supplemented with 0.1% HSA, and stored on ice until used in assays. Control U937 cells were preincubated with the LDV-containing small molecule for blocking. Before data acquisition, cells were warmed to 37°C for 10 min separately and then mixed. During data acquisition, the samples were stirred with a 5 × 2-mm magnetic stir bar (Bel-Art Products) at 300 rpm and kept at 37°C. For stimulation, indicated concentrations of fMLFF peptide ATP and U73122 were added. For stimulation using PMA, U937 cells were preincubated with 1 μM PMA for 10 min at 37°C to allow for maximum PMA response to be reached before mixing of U937 cells with B78H1/VCAM-1 cells. The number of cell aggregates containing U937 adherent to B78H1/VCAM-1 (red and green cofluorescent particles) was followed in real time. The percentage of aggregation was calculated as follows: percentage of aggregation = (number of aggregates/(number of aggregates + number of singlets of both U937 and B78H1)) × 100. In several experiments, initial rates of singlet cell depletion of U937 cells only (red fluorescent particles) were calculated by fitting depletion curves to the single exponential equation. From these data, the rate of singlet cell depletion was calculated for each time interval, and then, it was extrapolated to the initial time point at which cell mixing had occurred. Experiments were done using a FACScan flow cytometer and Cell Quest software (BD Biosciences).

Intracellular Ca^{2+} measurements

Intracellular Ca^{2+} was measured as described in detail (19). Briefly, U937 cells (5×10^6 cells/ml) were loaded with 1 μM fluo-4 AM for 30 min at 37°C in RPMI 1640. Next, cells were washed with dye-free warm RPMI 1640 and incubated for 30 min before the experiment. Cells were then resuspended in HEPES buffer and treated as described above with stimuli or inhibitors.

Statistical analysis

Curve fits and statistics were performed using GraphPad Prism (GraphPad). Each experiment was repeated at least three times. The experimental curves represent the mean of two or three independent runs. SEM was calculated using GraphPad Prism.

Results

Phorbol esters induce the high-affinity state of VLA-4, which is quantitatively similar to the state induced by the inside-out signal

The LDV-FITC probe was used to characterize the affinity of VLA-4 induced by PMA. Fig. 2*A* shows a typical real-time activation and dissociation experiment in which LDV-FITC was added to a cell suspension after 30 s of stirring, and cells were activated 3 min after the beginning of the experiment. Because the concentration of the LDV-FITC probe in this type of experiments (typically 4 nM) was lower than K_d for the resting state of the receptor and higher than K_d for the activated state, the transition from the low- to the high-affinity state was accompanied by additional binding of the probe. An excess of unlabeled competitor was added 4–7 min after activation. By fitting dissociation kinetics to single exponential curves, dissociation rate constants (k_{off}) corresponding to states of different affinity were extracted. For VLA-4 on unstimulated U937 cells, k_{off} ~0.06–0.1 s^{-1} was obtained (data not shown). This k_{off} corresponds to the resting receptor state (state 1; see Fig. 10*A*) (16, 17). For PMA-treated cells, k_{off} was in the range of 0.017–0.023 s^{-1}, which corresponded to the physiologically activated, by inside-out signaling, receptor state (see fMLFF activation; Fig. 2*A* (16, 17)). Thus, according to the dissociation rate analysis, phorbol ester induced the high-affinity state of VLA-4, and it was quantitatively similar to the state induced by activation through the FPR.

The kinetics of VLA-4 activation by PMA was strongly dose dependent (Fig. 2*B*). However, despite the difference in the initial slope of the binding curves after addition of PMA, the plateau of LDV-FITC binding was the same over more than three orders of magnitude of PMA concentration (0.5 nM–2 μM). The interpretation of this result is that the affinity state of VLA-4 after activation is largely independent of PMA concentration. As differing concentrations of the phorbol ester most likely vary its uptake rates, subsequent experiments were performed using high concentrations of PMA (0.5–1 μM).

PMA induces the high-affinity state without VLA-4 conformational unbending

To determine whether PMA produces a conformational unbending of VLA-4, we performed the FRET assay (Fig. 2, *C* and *D*, see *Materials and Methods*, Fig. 1 and Refs. 6 and 7). Cells were preincubated with the LDV-FITC probe. Fluorescence of the probe was quenched with octadecyl rhodamine B (R18). Then, cells were activated by fMLFF or PMA. DMSO was used as a negative control (labeled R18 only; Fig. 2*C*). Next, data from Fig. 2*C* were replotted by subtracting the baseline data (R18 only) from activated cell data. The data are normalized, assuming that average MCF value for FPR-activated cells is equal to 100%; therefore, the *y*-axis is labeled as "Donor fluorescence, % relative to fMLFF" (Fig. 2*D*). As shown previously, activation of the cells transfected with the nondesensitizing mutant of FPR (ΔST) (6) led to the rapid unquenching of the FITC signal, which was interpreted as a change in the distance of closest approach between the VLA-4 ligand binding site occupied by LDV-FITC and the membrane surface (Fig. 1). With PMA activation, no significant change in FRET fluorescence was detected for up to 15 min after stimulation. Thus, contrary to activation by FPR (state 2), phorbol ester induced a high-affinity state of VLA-4 without any detectable conformational unbending of the molecule (state 3; see Fig. 10*A*).

Increased intracellular Ca^{2+} is sufficient to induce the high-affinity unbent state of VLA-4 (state 2)

Phorbol esters activate conventional protein kinase Cs (PKCs) (24) by mimicking diacylglycerol in the absence of Ca^{2+} signaling. Because PMA induced VLA-4 affinity up-regulation without increasing intracellular Ca^{2+} concentration (Fig. 2*E*), we investigated the role of intracellular Ca^{2+} in regulating VLA-4 unbending. Previously, we showed that up-regulation of VLA-4 affinity can be achieved by treating U937 cells with Ca^{2+} ionophores, while chelation of intracellular Ca^{2+} with BAPTA prevented the VLA-4 affinity change (19). In this study, we have extended this

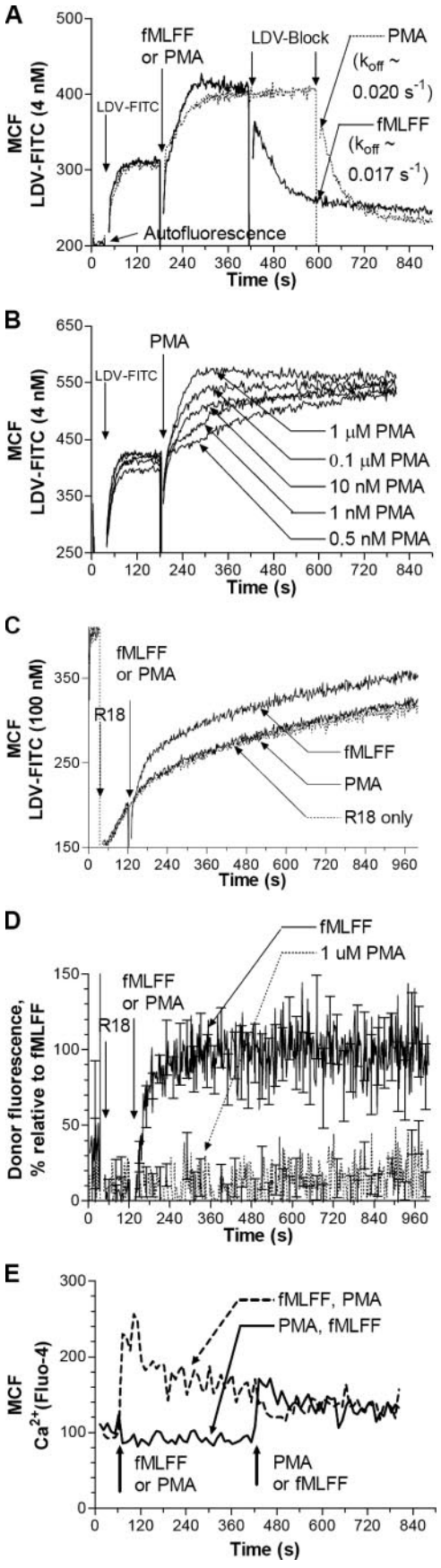

FIGURE 2. Binding and dissociation of the LDV-FITC probe on U937 cells; energy transfer on U937 cells between the LDV-FITC donor probe and octadecylrhodamine (R18) acceptor probe; and intracellular Ca^{2+} kinetics. Experiments were conducted as described under *Materials and Methods*. *A*, LDV-FITC probe binding and dissociation on U937 cells stably transfected with the nondesensitizing mutant of FPR (ΔST) (23) plotted as MCF vs time. The experiment involves sequential additions of fluorescent LDV-FITC probe (4 nM), fMLFF (100 nM, solid line), or PMA (100 nM, dashed), and nonfluorescent (2 μM) LDV-containing small molecule (arrows). The MCF value corresponding to cell autofluorescence is indicated by arrow. Dissociation rate constants (k_{off}) obtained by fitting dissociation curves to a single exponential decay equation are shown in parentheses. *B*, Response kinetics of LDV-FITC probe binding to U937 cells following stimulation by different concentrations of PMA (0.5 nM, −1 μM) plotted as MCF vs time. Experiments were performed as described in *A*. *C*, Real-time FRET unbending analysis on VLA-4 in response to inside-out signaling and PMA. U937 cells stably transfected with the nondesensitizing mutant of FPR (ΔST) (23) were preincubated at 37°C with 100 nM LDV-FITC probe to saturate low-affinity sites in HEPES buffer containing 1 mM Ca^{2+} and 1 mM Mg^{2+}. Next, LDV-FITC fluorescence was quenched after addition of 10 μM octadecyl rhodamine (R18, arrow). Then, cells were activated by addition of 100 nM fMLFF or 1 μM PMA. Data are plotted as MCF vs time for three conditions: quenched and then activated by fMLFF (solid line), quenched and then activated by PMA (gray solid line), and quenched only (R18 only, DMSO vehicle, dashed line). *D*, Normalized data from *C* processed as described in the text. SE is shown for every 20-s time point ($n = 2$). LDV-FITC probe binding and dissociation experiments, together with FRET experiments, were performed on the same day using the same cells and the same set of activating reagents. *E*, Kinetics of intracellular Ca^{2+} response detected using fluo-4 AM, after sequential additions of PMA (1 μM), followed by fMLFF (100 nM) (solid line), and fMLFF (100 nM), followed by PMA (1 μM) (dashed line), in U937 cells transfected with FPR (ΔST). Notice the absence of the signal increase (rather some decrease) after addition of PMA. One representative experiment of three experiments is shown.

observation by showing that the kinetics of the ionophore-induced affinity change was strongly dose dependent. At a low concentration of A23187 (10 μg/ml), up-regulation of VLA-4 affinity was transient; at a higher concentration (40 μg/ml), the high affinity was sustained for >10 min (Fig. 3*A*). Quantitatively, the affinity of VLA-4 induced by Ca^{2+} ionophores was very similar to the state induced by fMLFF or PMA activation (k_{off} ~0.019–0.023 s^{-1}). Thus, an increase in the intracellular Ca^{2+} concentration was sufficient to induce high-affinity VLA-4, which was quantitatively similar to the state induced by inside-out activation.

Next, to probe VLA-4 conformational unbending, we performed the FRET assay (Fig. 3*B*). We found that the overall kinetics of the conformational unbending was different for activation using A23187 in comparison to fMLFF. Two distinct waves of molecular unbending can be seen. A rapid, transient (~1 min) conformational unbending of VLA-4 after ionophore addition was followed by a slow conformational unbending over the next 8–10 min. Biphasic kinetics for intracellular Ca^{2+} concentration reflect an initial rise of intracellular Ca^{2+} induced by ionophore and activation of Ca^{2+} pumps that actively remove calcium from the cytoplasm. If the Ca^{2+} influx is higher than the pump's capacity, intracellular Ca^{2+} slowly rises over time. It is worth noting that, at the end of the experiment with A23187, the FRET signal went approximately to the level of the formyl peptide-activated cells. This result suggests that the distance of closest approach between the ligand binding site and the membrane (r_c in Fig. 1) was the same for both cases. Therefore, the affinity state and the conformational unbending of VLA-4 induced by ionophore were similar to the state induced by FPR stimulation (state 2; see Fig. 10*A*).

Addition of Ca^{2+} ionophore to PMA-activated cell results in the rapid conformational unbending of the molecule

To investigate the role of intracellular Ca^{2+} in the regulation of VLA-4 conformational unbending, we also treated PMA-activated

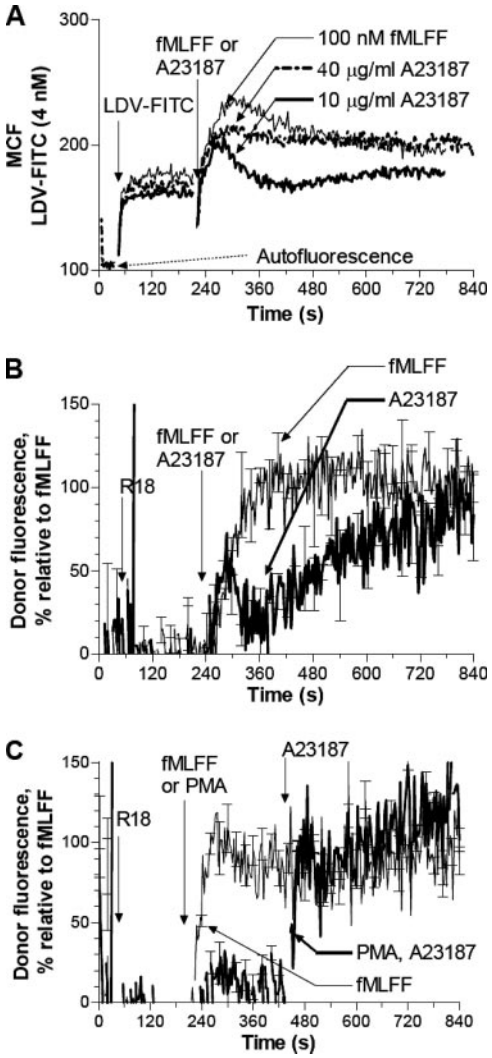

FIGURE 3. Response kinetics of LDV-FITC probe binding to U937 cells following stimulation by fMLFF and Ca^{2+} ionophore (A23187); energy transfer on U937 cells between LDV-FITC donor probe and octadecylrhodamine (R18) acceptor probe. *A*, Response kinetics of LDV-FITC binding to U937 cells transfected with the nondesensitizing mutant of FPR (ΔST) following stimulation by fMLFF and A23187 are plotted as MCF vs time. The experiment involved sequential additions of LDV-FITC (4 nM), fMLFF (100 nM), or A23187 (10–40 μg/ml). The MCF value corresponding to the cell autofluorescence is indicated by arrow. *B*, Real-time FRET experiments are as described in Fig. 2*C*, except that A23187 (40 μg/ml, solid line) was used to activate VLA-4. *C*, Real-time FRET experiments are as described in Fig. 2*D*, except cells treated with PMA (1 μM) were treated additionally with A23187 (40 μg/ml) (PMA, A23187, solid line). Data were processed as described for Fig. 2, *C* and *D*, and therefore, the *y*-axis labeled as "Donor fluorescence, % relative to fMLFF." The positive control (fMLFF, 100 nM) is also shown. Curves are means of two independent runs calculated on a point-by-point basis. SE is shown for every 20-s time point ($n = 2$).

cells with Ca^{2+} ionophore (Fig. 3*C*). This treatment resulted in a very rapid increase of the signal that reached the same plateau as stimulation by formyl peptide alone. As with ionophore alone, this suggested that conformational unbending of the molecule was similar in both cases (r_c was about the same; Fig. 1). However, the overall kinetics of cell activation by A23187 in the presence of PMA was different than for A23187 alone. The initial rate of signal increase was faster for the case of PMA plus A23187, and two-wave behavior was practically absent (compare PMA and A23187, solid line, Fig. 3*C* to A23187 only, solid line, Fig. 3*B*, with formyl peptide in both panels). Thus, an increase in intracellular Ca^{2+} was sufficient to induce the high-affinity unbent state of VLA-4 whereas activation of PKC alone using PMA in the absence of cytoplasmic Ca^{2+} elevation was not. Therefore, elevation of cytoplasmic Ca^{2+} is essential for the induction of the unbent state of VLA-4.

U-73122 rapidly down-regulates VLA-4 affinity in cells activated through FPRs

To investigate the role of downstream signaling in the regulation of VLA-4 activation by FPRs, we used the putative phospholipase C (PLC) inhibitor U-73122 to block the signaling pathway from FPRs toward VLA-4. Preincubation with U-73122 completely blocks integrin activation through FPRs (Fig. 4*A*, dotted line). Moreover, VLA-4 affinity up-regulation can be reversed in real time in a dose-dependent manner (Fig. 4*B*).

Increasing intracellular Ca^{2+} with Ca^{2+} ionophore is not sufficient to restore down-regulated VLA-4 affinity after addition of U-73122

FPR/ΔST activation results in a sustained high affinity and relatively sustained Ca^{2+} response (Fig. 5, *A* and *C*). A rapid decrease in VLA-4 affinity in cells treated with U-73122 was accompanied by a decrease in intracellular Ca^{2+} as detected by fluo-4 (Fig. 5, *B* and *D*). The kinetics of LDV-FITC probe dissociation and the fluo-4 signal decrease after addition of U-73122 were almost identical (compare fluo-4 in Fig. 5*B* and LDV-FITC in Fig. 5*D* after U-73122 addition). The subsequent addition of A23187 resulted in a full Ca^{2+} elevation. In fact, the peak of the fluo-4 fluorescence signal was slightly higher than for formyl peptide. However, in this case, elevated intracellular Ca^{2+} was insufficient to increase VLA-4 affinity, and the LDV-FITC probe-binding signal did not recover to the level of activated cells (Fig. 5, *B* and *D*, after A23187 addition). Thus, U-73122 blocked a signaling step that was obligatory for affinity up-regulation that cannot be restored by Ca^{2+} elevation.

Increase of intracellular Ca^{2+} by Ca^{2+} ionophore is sufficient to restore VLA-4 conformational unbending after addition of U-73122

To investigate whether U-73122 affects the conformational unbending of VLA-4, we performed the FRET-unbending assay in which cells were treated sequentially with U-73122 and A23187 (Fig. 6*A*). Addition of U-73122 to cells previously activated with formyl peptide led to rapid loss of conformational unbending, which recovered spontaneously to ~50% of the positive control by the end of the experiment (Fig. 6*A*, fMLFF and U-73122 (dotted line)). The kinetics of the intracellular Ca^{2+} elevation in this case also showed a rapid and transient decrease with a slow recovery phase (data not shown). Addition of A23187 induced rapid conformational unbending, reaching 100% of the positive control within 3 min (Fig. 6, fMLFF, U-73122, and A23187 (solid line)). This concentration of A23187 was sufficient to rapidly elevate the intracellular Ca^{2+} level on a similar timescale (Fig. 5*B*).

Preincubation with U-73122 blocks only VLA-4 affinity change but not the molecular unbending and Ca^{2+} response

To further investigate the effect of U-73122 upon VLA-4 activation, we preincubated cells with 1 μM U-73122 for 10 min. Next, cells were activated using formyl peptide. In these conditions, the VLA-4 affinity change was completely blocked (Fig. 6*B*), although molecular unbending and Ca^{2+} elevation were not affected (Fig. 6, *C* and *D*). In fact, the Ca^{2+} level was

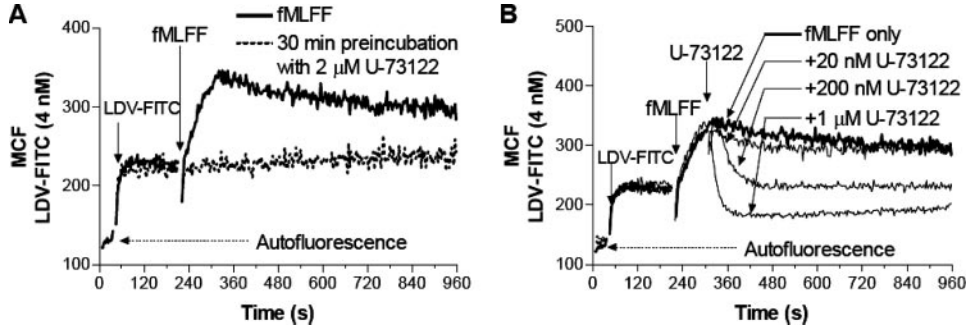

FIGURE 4. Response kinetics of LDV-FITC probe binding to U937 cells following treatment with fMLFF and PLC inhibitor U-73122. *A*, U937 cells transfected with FPR (ΔST) were preincubated for 30 min with 2 μM U-73122 (dashed line) or 2 μl of DMSO (solid line) at 37°C. Next, LDV-FITC probe (4 nM) and fMLFF (100 nM) were sequentially added. *B*, U937 cells transfected with FPR (ΔST) were sequentially treated with LDV-FITC probe (4 nM), fMLFF (100 nM), and different concentrations of U-73122. Data are plotted as MCF vs time. The MCF value corresponding to the cell autofluorescence is indicated by arrow.

slightly higher for U-73122-treated cells. This result additionally supports the idea that the affinity change is regulated independently from the conformational unbending, and it is independent upon Ca^{2+} signaling. On the contrary, the kinetics of integrin conformational unbending was similar to the kinetics of intracellular calcium in all experiments. For the case of the real-time addition of U-73122, a rapid decrease in the intracellular calcium was transient, and it slowly recovered very similar to the FRET signal (Fig. 6*A* and data not shown). For preincubation experiments, compare Fig. 6, *C* and *D*. Taken together with the fact that addition of Ca ionophore facilitates integrin conformational unbending (Figs. 3*C* and 6*A*), our data suggest that Ca elevation plays an important role in the regulation of integrin conformational unbending.

The kinetics of VLA-4 molecular unbending after GPCR activation is different from the kinetics of affinity change

Next, to compare the real-time kinetics of affinity change and integrin conformational unbending, we took advantage of the P2Y (purinergic) receptors constitutively expressed on U937 cells (25), which were stably transfected with nondesensitizing mutant of FPRs (23). Formyl peptide activation served as a positive control. The VLA-4 affinity change detected in the ligand-binding assay was very rapid and reversible (Fig. 7*A*). The signal returned to a baseline value within ~200 s after ATP activation. However, the FRET signal did not return to the baseline after >12 min (Fig. 7*B*). By the end of the experiment, it reached ~50% of the positive control (Fig. 7*B*, fMLFF, dotted line). These partial quenching results do not distinguish whether all VLA-4 molecules were still partially unbent (intermediate extended state) long after the affinity of the binding pocket had returned back to the resting state or whether a fraction of the VLA-4 molecules was still extended, whereas the rest of the integrins returned back to the bent conformation (Fig. 1). As shown above, the conformational unbending of VLA-4 seems to be related to the intracellular Ca^{2+} concentration (Figs. 5 and 6). Therefore, we compared the kinetics of VLA-4 conformational unbending and intracellular Ca^{2+} detected using fluo-4 (Fig. 7*C*). Both the FRET signal and the intracellular Ca^{2+} concentration peaked very rapidly and did not return to the

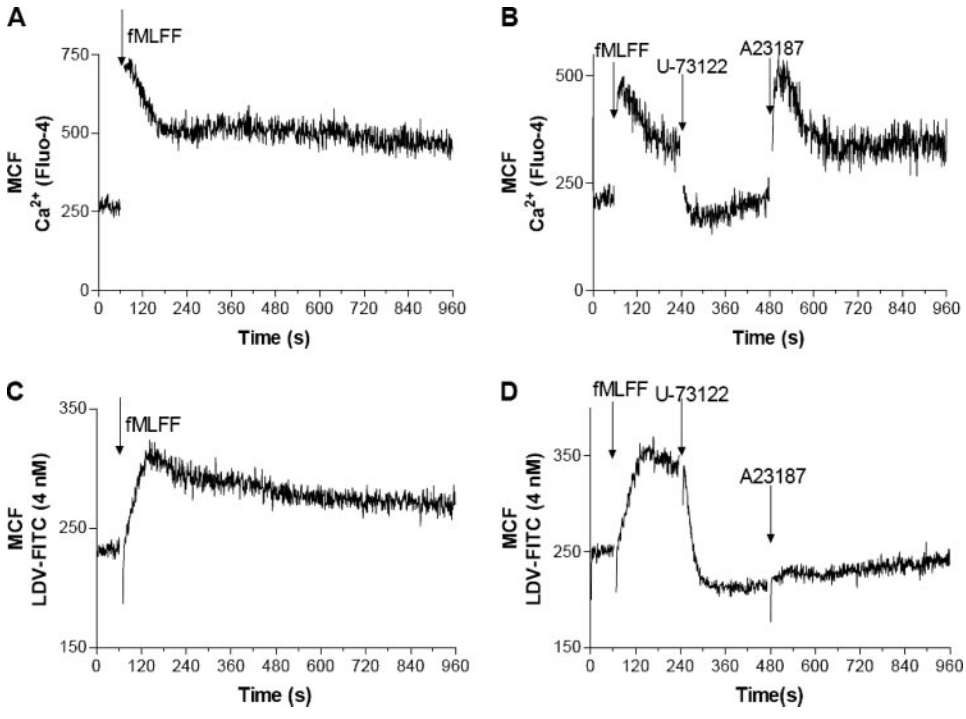

FIGURE 5. Kinetics of intracellular Ca^{2+} response, detected using fluo-4, AM; LDV-FITC probe binding and dissociation following cell treatment by fMLFF, PLC inhibitor U-73122, and Ca^{2+} ionophore A23187. *A*, Kinetics of fluo-4 signal changes in response to the fMLFF activation of U937 cells transfected with FPR (ΔST). *B*, Kinetics of fluo-4 signal changes after sequential addition of fMLFF (100 nM), U-73122 (1 μM), and A23187 (40 μg/ml). *C*, Response kinetics of LDV-FITC probe binding to U937 cells following stimulation by fMLFF, or *D*, after sequential addition of fMLFF (100 nM), U-73122 (1 μM), and A23187 (40 μg/ml). Before the stimulation cells in (*C* and *D*) were preincubated with 4 nM LDV-FITC probe for 5 min at 37°C. Data are plotted as MCF vs time.

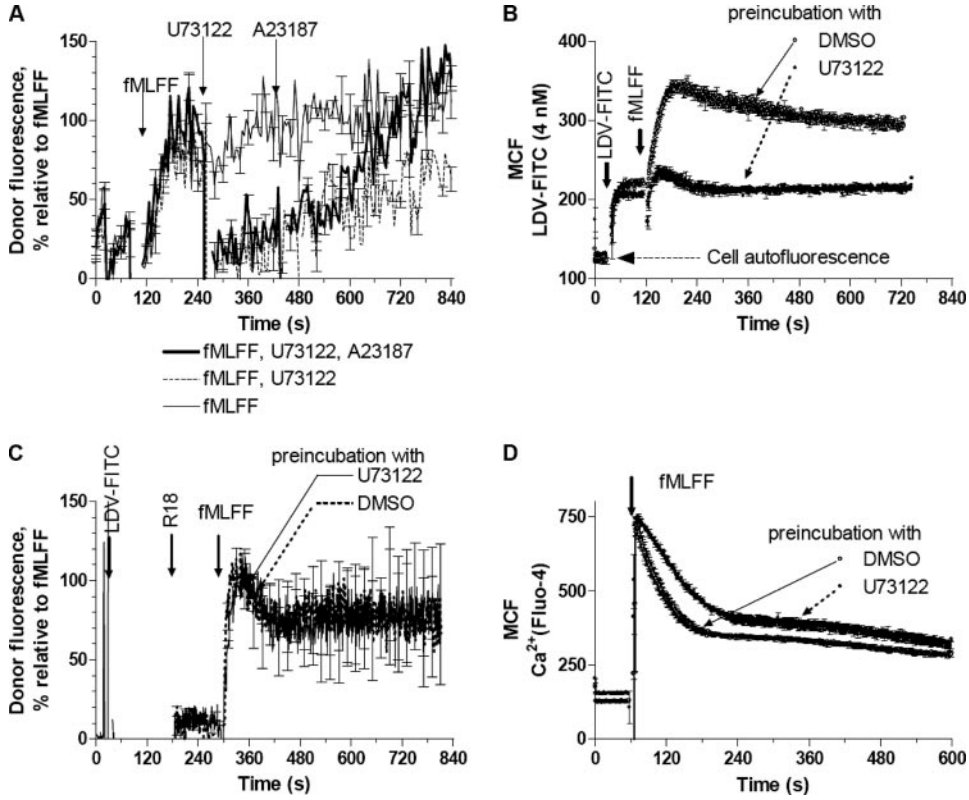

FIGURE 6. Effect of U-73122 on the kinetics of energy transfer, LDV-FITC probe binding, and kinetics of intracellular Ca^{2+} response following stimulation with fMLFF in U937 cells transfected with FPR (ΔST). *A*, Kinetics of the FRET signal change after sequential addition of fMLFF (100 nM), U-73122 (1 μM), and in the presence or absence of A23187 (40 μg/ml). The positive control (100 nM fMLFF) is also shown. Data were processed as described for Fig. 2, *C* and *D*, and therefore, the *y*-axis labeled as "Donor fluorescence, % relative to fMLFF." *B–D*, Cell were preincubated with 1 μM U-73122 for 10 min at 37°C. Control cell were preincubated with DMSO. *B*, Response kinetics of LDV-FITC probe binding to U937 cells following treatment with fMLFF. Cells were treated sequentially with LDV-FITC probe (4 nM) and fMLFF (100 nM). *C*, Real-time FRET experiments are as described in Fig. 2*D*, except cells treated with fMLFF (100 nM). Data were processed as described for Fig. 2, *C* and *D*, and therefore, the *y*-axis labeled as "Donor fluorescence, % relative to fMLFF." *D*, Kinetics of intracellular Ca^{2+} response, detected using fluo-4, AM; after addition of fMLFF (100 nM). *A* and *B*, SE is shown for every 20-s time point ($n = 2$). *C* and *D*, SE is shown for every point ($n = 3$). Experiments shown on *B–D* were performed on the same day using the same cells and the same set of reagents.

baseline value even at the end of the experiment (compare solid lines in Fig. 7, *B* and *C*). Thus, in these experiments, as for the experiments with Ca^{2+} ionophore and U-73122, the kinetics of the molecule conformational unbending was also similar to the kinetics of the intracellular Ca^{2+}. This result raises the possibility that the integrin affinity change and conformational unbending can have different thresholds for intracellular Ca^{2+}: the affinity change requires much higher Ca^{2+} concentration.

A similar relationship between the kinetics of the FRET and affinity change response has been observed for CXCR4-transfected U937 cells (data not shown) and wild-type FPRs (see Fig. 4*B* in Ref. 6 and Fig. 4*B* in Ref. 16). These data indicate that the conformational unbending of VLA-4 and the affinity state of the binding pocket are regulated in a different temporal fashion, supporting the idea that conformational unbending and affinity are regulated by different mechanisms. Taken together, our data suggest that the affinity state of VLA-4, detected in a small ligand-binding assay, and the conformational unbending of the molecule, detected using the FRET based assay, are regulated by two related but distinct signaling pathways. Nominally, PKCs and the diacylglycerol-related pathway, which can be activated by PMA, regulate affinity, whereas the Ca^{2+}-dependent pathway regulates both molecular unbending and affinity (presumably through Ca^{2+}-dependent PKCs).

Rapid modulation of integrin affinity leads to rapid modulation of cell aggregation

To study the role of VLA-4 affinity and conformational unbending in the regulation of cell aggregation, we performed a VLA-4/VCAM-1-specific real-time cell adhesion assay (Fig. 8). The rate of aggregate formation in these types of suspension assays has been related to the efficiency with which a cell collision results in the formation of a stable aggregate (26). The specificity of cell aggregation was tested using anti-α_4 integrin mAb (HP2/1) (17), as well as the unlabeled LDV small molecule that completely blocked cell aggregation (Fig. 8*A*). As shown previously, cell aggregation as detected using cell aggregates (red and green cofluorescent particles; see *Materials and Methods*) did not discriminate between doublets and higher order aggregates (27). Therefore, the more rigorous analysis of cell aggregation was done by using singlet cell depletion methodology (28).

As shown previously, rapid up-regulation of VLA-4 affinity on U937 cells through GPCRs resulted in the rapid cell aggregation. Rapid and reversible change in the integrin affinity induced by ATP resulted in transient increase in the aggregation kinetics (Fig. 8*A*). The initial phases of cell aggregation after activation were very similar for the case of aggregates and singlet cell depletion (compare curves on Fig. 8*B*).

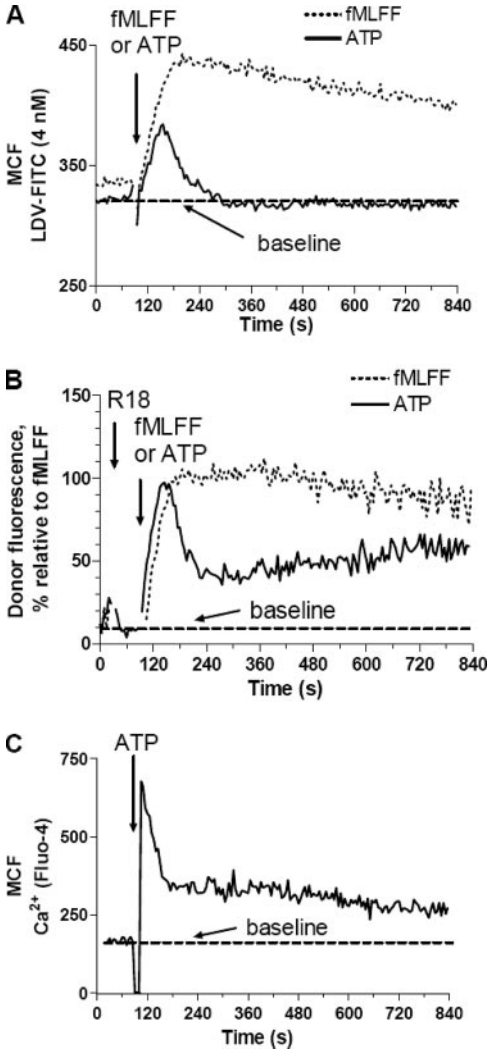

FIGURE 7. Real-time kinetics of VLA-4 affinity change, energy transfer, and intracellular Ca^{2+} response after activation of purinergic receptors constitutively expressed on U937 cells (25) transfected with FPR (ΔST). *A*, Response kinetics of LDV-FITC probe binding to U937 cells following treatment with ATP or fMLFF (positive control). Before the experiment, cells were preincubated with 4 nM LDV-FITC probe for 5 min at 37°C. Data are plotted as MCF vs time. *B*, Kinetics of the FRET signal change after addition of ATP (10 μM). The positive control (100 nM fMLFF) is also shown. Data were processed as described for Fig. 2, *C* and *D*, and therefore, the *y*-axis labeled as "Donor fluorescence, % relative to fMLFF." *C*, Kinetics of intracellular Ca^{2+} response, detected using fluo-4, AM, as described in *Materials and Methods*. The baseline value (dashed line) represents the mean value before addition of the stimuli. Data are plotted as MCF vs time. Representative experiments of three independent experiments are shown.

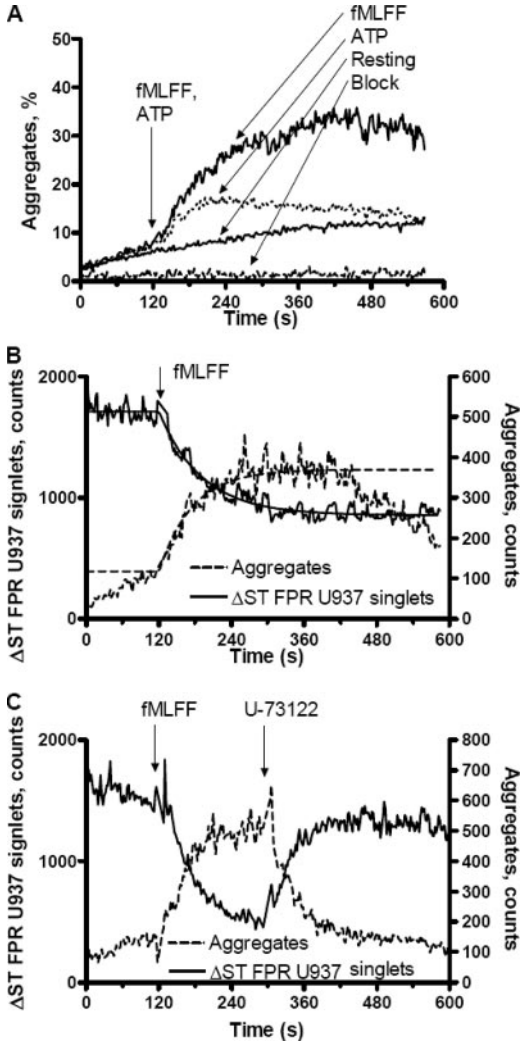

FIGURE 8. Changes in cell adhesion between U937 FPR (ΔST) and VCAM-1-transfected B78H1 cells at resting state and in response to receptor stimulation. *A*, Data are plotted as percentage of aggregates vs time. Four different experimental conditions are shown (resting state (no stimulus), stimulation with 100 nM fMLFF, stimulation with 1 μM ATP, and preincubation with blocking LDV small molecule). The nondesensitizing FPR mutant is used to maintain VLA-4 in a state of constant affinity. *B*, Data are plotted as aggregates and U937 FPR (ΔST) singlets vs time. Singlet depletion curve exhibited a single exponential kinetics. *C*, The effect of PLC inhibitor U-73122 upon cell adhesion. Data are plotted as aggregates and U937 FPR (ΔST) singlets vs time. Small arrows indicate the moment of stimulus addition. Representative experiments of three independent experiments are shown.

Moreover, termination of signaling using U-73122, which in the LDV-FITC-binding assay shows rapid and sustained down-regulation of VLA-4 affinity (Fig. 4), resulted in a very rapid cellular disaggregation as detected in both cell aggregation and singlet cell depletion protocols (Fig. 8*C*). Thus, in agreement with previous reports, the affinity of the VLA-4-binding pocket dramatically affects the cell adhesion avidity in a VLA-4/VCAM-1-specific adhesion model system, primarily by regulating the lifetime of the aggregate (17, 27). However, because U-73122 caused both affinity down-regulation (Fig. 5) and rapid integrin bending (Fig. 6*A*), it is impossible to draw any conclusion about the role of integrin conformational unbending in U-73122-induced cellular disaggregation (Fig. 8*C*). It is possible that integrin low affinity and bending can both participate in the induction of disaggregation: low affinity—by decreasing the life-time of VLA-4/VCAM-1 bonds, and bending—by masking previously exposed binding site and thereby lowering the probability of bond reengagement.

The initial rate of cell aggregation is regulated by VLA-4 conformational unbending

Finally, to investigate the role of VLA-4 conformational unbending, we have studied the real-time kinetics of cell aggregation using singlet cell depletion methodology (Fig. 9; Ref. 28). To generate the high-affinity bent state of VLA-4, U937 cells were preincubated with a high concentration of PMA for

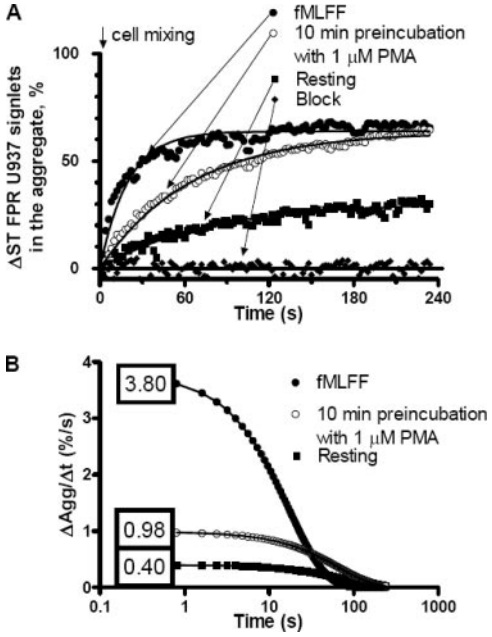

FIGURE 9. Estimation of the initial rate of cell aggregation between U937 FPR (ΔST) and VCAM-1-transfected B78H1 cells. *A*, Singlet cell depletion data as shown on a Fig. 8*B* were normalized assuming that average singlets count for blocked sample is equal to 0%, and 0 singlet count is equal to 100% (no singlets left in solution, therefore all cells are in the aggregates); therefore, the *y*-axis is labeled as "ΔST FPR U937 singlets in the aggregate, %." Four different experimental conditions are shown (resting state (no stimulus), stimulation with 100 nM fMLFF added at the time of the cell mixing, stimulation with 1 μM PMA for 10 min at 37°C before cell mixing (this time is sufficient to generate high-affinity state of VLA-4 (Fig. 2*B*)) and preincubation with blocking LDV small molecule). Curves show a single exponential fit to the data. *B*, Estimation of the initial rate of cell aggregation. Using the curve fits from *A*, the absolute rates of the cell aggregation (percentage of cell singlet incorporated into the aggregate per second) were calculated for each time interval and plotted vs time. The initial rate of the cell aggregation extrapolated to the time 0 point is shown next to each curve. Representative experiment of four independent experiments is shown.

10 min at 37°C, and to generate the same high affinity but unbent state, cells were activated by fMLFF. The aggregation results demonstrate dramatically different initial rates of singlet cell depletion for the cases of PMA and fMLFF activation, despite the fact that the steady-state values of cell aggregation were very similar (compare open and filled circles on Fig. 9*A* at 200–240 s after cell mixing). The initial rates of cellular aggregation were significantly greater for the fMLFF-induced unbent conformation than the bent conformations of the resting state or the PMA-activated state (compare squares and open circles to filled circles; Fig. 9*B*). Thus, our data suggest that conformational unbending of VLA-4 primarily affects the initial rate of cell aggregation, and the aggregation rate is largely independent of the affinity state of the binding pocket (as shown in Fig. 2*A*, the resting and PMA-activated states have similar off-rates (k_{off}) for the VLA-4 ligand). It appears that the exposure of the VLA-4 binding site through conformational unbending changes the adhesive efficiency of cell collisions. In contrast, the overall number of aggregates appears to depend upon the lifetime of the aggregate, which is determined by the affinity of the VLA-4-binding pocket when there is a small number of VLA-4/VCAM-1 bonds (27).

Discussion

The VLA-4/VCAM-1 model system

Undifferentiated U937 cells are known to possess all the intracellular signaling apparatus and machinery necessary to generate a motile phenotype when stably transfected with a chemoattractant receptor (20). These suspension cells constitutively express VLA-4, and like a majority of peripheral blood leukocytes at rest, they exhibit a nonadhesive phenotype with a low affinity state of VLA-4 (16). The affinity can be rapidly up-regulated through an inside-out signaling pathway, and the kinetics of the affinity change reflects the signaling properties of a particular GPCR, such as their activation and desensitization kinetics (7, 16). Also, no significant "outside-in" signaling or intracellular Ca^{2+} elevation is detected in U937 cells in response to the binding of LDV containing small molecule alone. Human peripheral blood lymphocytes during activation through different GPCRs have demonstrated VLA-4 affinity states that were quantitatively similar to U937 cells. The use of B78H1 mouse melanoma cells stably transfected with human VCAM-1 together with U937 cells creates a unique VLA-4/VCAM-1 specific cellular adhesion system, which was previously used to study aggregation and disaggregation kinetics on live cells in real-time after activation (17, 27). Thus, this model system seems to be relevant to the role of VLA-4 affinity and conformational unbending in the regulation of cell adhesion in a relevant human myeloid cell.

Integrin affinity, conformational unbending, and cell adhesion

VLA-4 has the potential to exhibit multiple affinity states that mediate tethering, rolling and arrest on its endothelial ligand, VCAM-1 (12, 29–31). Previously, we have used the LDV-FITC probe as a model ligand that reports the affinity state of VLA-4 under different activating conditions (16), and our data suggested that the VLA-4 affinity state strongly correlated with the degree of molecular unbending detected using FRET (6, 7). Here, using activators and inhibitors of cell signaling we report the discordance between the high affinity state of VLA-4 as measured by the ligand binding/dissociation assay and the conformational unbending of the molecule in a FRET assay (Fig. 10*A*). Affinity change and conformational unbending also exhibit different kinetics after receptor activation (Fig. 7).

In several experimental systems, phorbol esters have been shown to increase cell adhesion avidity. This result was attributed to changes in the lateral mobility of the integrin (32), change in the affinity after stimulation detected using soluble VCAM-1 (33), or absence of the affinity change of VLA-4 induced by "inside-out signal" (34). Our results support the idea that phorbol esters do in fact up-regulate affinity of VLA-4 for ligand in a time and dose dependent manner. Thus, while phorbol esters up-regulate affinity on a relevant time scale that is similar to the affinity of "physiologically" activated VLA-4 (state 2; Fig. 10*A*), VLA-4 does not extend in response to PMA as detected using the FRET assay (Fig. 2, *C* and *D*).

The absence of a change in FRET in PMA treated cells (Fig. 2, *C* and *D*), together with the up-regulation of the binding affinity (Fig. 2, *A* and *B*), points to the possibility of a localized conformational change that affects only the affinity of the LDV-binding pocket without a large conformational rearrangement and conformational unbending of the molecule (state 3; Fig. 10*A*). A recently published model of a fibronectin fragment bound to the $\alpha_V\beta_3$ integrin in a bent form supports the possibility of this scenario (5). However, the proximity of the ligand-binding pocket to the membrane in a bent form could presumably reduce the initial phases of cell recruitment, such as tethering and rolling. Our aggregation

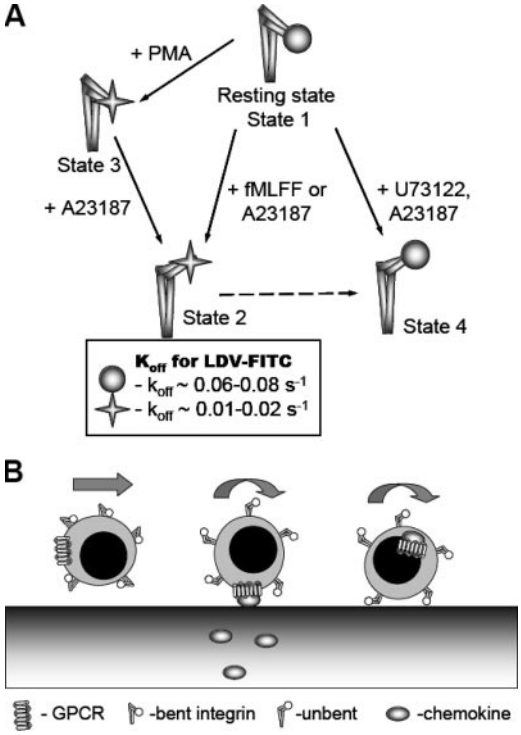

FIGURE 10. Schematic diagram of VLA-4 activation states and possible model of leukocyte recruitment and rolling regulation by unbent integrin conformation. *A*, Activation through GPCR led to both affinity up-regulation and conformational unbending of VLA-4 integrin (state 2). The affinity state remained up-regulated for the cells transfected with the non-desensitizing mutant of FPR ΔST that is lacking all serine and threonine phosphorylation sites within the C terminus (23). For wild-type GPCRs, affinity up-regulation was rapid and transient. After the affinity of the binding pocket has returned to the resting state, a fraction of the integrins remained unbent. This generated a low-affinity unbent state similar to state 4 (dashed arrow). Activation by PMA resulted in high affinity without conformational unbending (state 3). Addition of A23187 to PMA-activated cells produced rapid conformational unbending of the molecule (similar to state 2). Treatment of GPCR-activated cells (state 2) with PLC inhibitor U-73122 resulted in a rapid, sustained down-regulation of integrin affinity and loss of conformational unbending (similar to the resting state 1). Conformational unbending but not low affinity was reversed by addition of A23187 (state 4). Different shapes for the VLA-4 head group represent different affinity states of the ligand-binding pocket as determined by dissociation rate (k_{off}) of the LDV-FITC probe. The conformational unbending representation is not drawn to scale. *B*, Possible scenario for regulation of leukocyte recruitment and rolling by long-lived conformational unbending of integrins. After localized exposure to chemokines on endothelial cells and rapid and reversible affinity change, a fraction of integrins remained in an unbent conformation. This unbent state with low affinity of the binding pocket would facilitate recruitment and rolling of leukocytes as was shown recently for LFA-1 integrin (11).

experiments presented in the current report directly support this idea. Despite the fact that affinity state of the VLA-4 binding pocket was identical for the case of PMA and fMLFF activation (compare two off-rates (k_{off}), Fig. 2*A*), the initial rate of cell aggregation after fMLFF activation was three to four times faster (Fig. 9). Taking into the account that the lifetime of the aggregate is determined by the affinity between VLA-4 and VCAM-1 (17, 27), we interpret the difference in the initial rate of aggregation as a result of molecular unbending, which dramatically changes the efficiency of the cellular aggregation. Moreover, because at the moment of cell mixing (time 0 s of aggregation kinetics; Fig. 9) the number of aggregates is equal to 0, we can compare the initial aggregation rate for the resting low affinity state to the activated states. Based on the data obtained in the FRET unbending assay after activation by PMA, VLA-4 remains in the bent conformation (Fig. 2). Thus, the difference in the initial aggregation rates between resting and PMA activated states (~2-fold or less) was significantly smaller than the difference between PMA and fMLFF activated cells (~4-fold; Fig. 9*B*) and is consistent with the principal role of VLA-4 molecular unbending in the regulation of initial aggregation rate (and presumably initial cell capture and recruitment, such as cell tether frequency). Several reports from other laboratories could be re-evaluated in terms of this new model.

Thus, according to the rolling and tethering data of Grabovsky et al. (2) for lymphocytes in a flow chamber, GPCR and PMA modulate VLA-4 tether properties through distinct mechanisms. The authors found that the chemokine CXCL12 supported a 3-fold higher frequency of VLA-4 tethers, whereas the tether frequency for PMA-treated cells was unchanged. In addition, PMA prolonged the lifetime of the tethers, which was interpreted as a change in the dissociation rate of the VLA-4/VCAM-1 bond. The authors concluded that chemokines up-regulate VLA-4 avidity to VCAM-1 through distinct pathways from those implicated in VLA-4 stimulation by phorbol ester (2). Data presented in this article suggest that PMA fails to induce the conformational unbending of VLA-4, a result that could account for the difference in tether frequency between phorbol ester and chemokines (2).

According to the findings of Adair et al. (5), an integrin heterodimer in a bent conformation can stably bind its native ligand. Thus, a local conformational change in the ligand-binding pocket even in the absence of conformational unbending would account for the increased affinity and prolonged tether lifetime. In contrast, the conformational unbending of the integrin, which presumably exposes the VCAM-1 binding site because of the headpiece rotation (and therefore facilitate encounters between integrin and its ligand) might account for an increase in the tether frequency. Conformational unbending of the integrin molecule could facilitate both tethering and rolling as recently reported for $\alpha_L\beta_2$ integrin (11).

Another notable finding, that a significant fraction of integrins remain unbent long after the affinity state of the binding pocket had returned to the resting state (Fig. 7) provides a potential explanation for the higher frequency of VLA-4 tethers observed without a significant change in the tether lifetime (see Fig. 4*C* in Ref. 2). This long-lived conformational unbending of integrins would provide a fundamental mechanism for increased capture and rolling after leukocytes encountered chemokines but failed to arrest on endothelium during transient up-regulation of affinity. We propose that the low affinity unbent conformation of integrins could represent a tethering state of primed leukocytes (Fig. 10*B*).

Integrin extension or conformational unbending

Previously we reported that according to the FRET measurements the distance of the closest approach between the LDV-FITC binding pocket and the membrane changed from ~25 to ~75 Å depending upon activation stimuli (6, 7). As the length of fully extended integrin is ~200 Å, the interpretation of FRET measurements depends on whether all VLA-4 integrins respond to the inside-out signaling and the exact position of the resting integrin. As flow cytometry measurements are averaged on an individual cell basis, we do not measure the fraction of integrins that unbent nor do the FRET measurements provide a definitive determination of full extension.

It is generally accepted that integrin extension (unbending) is a part of the inside-out activation mechanism, which eventually leads to a high-affinity "activated" integrin conformation (8). Our

previous affinity state measurements suggested that affinity responses are nearly homogeneous (see Fig. 5 in Ref. 16). However, the data presented in the current report suggest that the conformational unbending of the integrin is not intrinsically related to the affinity state of the binding pocket. Thus, it is possible that the conformational unbending response could be heterogeneous, and the number of participating integrins could be <100%. In this case a small fraction of fully extended integrins would show the same signal change as a big fraction of partially unbent molecules, and currently we do not have any way to discriminate between these two possibilities. Thus, reported changes in the distance of closest approach represent a lower estimate, which is based on the assumption that integrin head group is within 25 Å from the membrane at resting state, and that all 100% integrins responded and assumed exactly the same conformation. Furthermore, our data do not discriminate between different models of integrin activation (switchblade, deadbolt, angle-poise (10, 35, 36)) because FRET measurements only report the average distance of closest approach between the binding site for LDV-FITC ligand and the cell membrane.

Is there a relationship between intracellular calcium and integrin conformational unbending?

Phorbol esters induce activation of conventional diacylglycerol-dependent PKCs without a significant elevation of intracellular calcium. Elevation of intracellular calcium by itself was sufficient to induce the high affinity unbent state of VLA-4 (Fig. 3, *A* and *B*). Addition of ionophore to PMA-treated cells resulted in the rapid unquenching of the FRET signal up to the level of formyl peptide treatment (Fig. 3*C*). This led us to hypothesize that cytoplasmic Ca^{2+} elevation is obligatory for molecular unbending, in contrast to the diacylglycerol dependent PKC activation, which regulates the affinity of ligand binding only. A number of reports correlate PKC-dependent signaling to integrin signaling and cell migration (37, 38). We anticipated that the PLC inhibitor U-73122, which is known to rapidly block GPCR signaling and cytosolic calcium elevation (39), would block the conformational change of VLA-4. In fact, U-73122 pretreatment blocked the affinity change (Fig. 4*A*) and down-regulated VLA-4 affinity in real-time (Fig. 4*B*). In addition, we found that U-73122 induced a sharp decrease in intracellular Ca^{2+} in formyl peptide activated cells as detected by fluo-4, and that this decrease could be reversed by addition of Ca^{2+}-ionophore (Fig. 5*B*). However, despite the fact that the fluo-4 signal, after addition of Ca^{2+} ionophore, was higher than the first peak induced by formyl peptide, LDV-FITC binding affinity was not re-established (Fig. 5*D*). We examined in parallel the conformational regulation of VLA-4 by U-73122. Although the inhibitor produced a rapid reversal of the conformational unbending as well as LDV-FITC binding, Ca^{2+} ionophore completely restored the conformational unbending (Fig. 6). Moreover, the overall kinetics of the conformational unbending after addition of Ca^{2+} ionophore in the presence of U-73122 was similar to the kinetics in the absence of U-73122 (compare sold lines in Fig. 6 with Fig. 3*B*). Biphasic kinetics was observed in both cases. Because U-73122 blocked VLA-4 affinity up-regulation in both calcium as well as via PMA (data not shown) dependent pathways, it is possible that there is a specific role for PLC in VLA-4 affinity regulation. Taken together, our data suggest that the conformation of the ligand binding pocket and the conformational unbending of the molecule are regulated through distinct mechanisms. Pocket conformation, as reported by LDV-FITC binding and dissociation, depends at least in part upon the PKC pathway, while molecule unbending depends at least in part upon elevated intracellular calcium. The role of PLC is currently uncertain.

It is worth noting that the amplitude of the conformational unbending signal was always similar to that observed for formyl peptide induced activation. Ca^{2+} ionophore alone, or in the presence of PMA or U-73122 induced the same relative change despite the difference in the conformational unbending kinetics. This suggests that the distance of closest approach (r_c; Fig. 1) was similar and that the conformational unbending induced by inside-out signaling receptors is independent of the activating receptor, similar to what we had seen with the affinity state of the binding pocket (16). However, if the change in integrin affinity after phorbol ester treatment occurs without conformational unbending of the molecule, it suggests that several different proteins could participate in the "inside-out" activation of the integrins; some of them would regulate affinity, others – the conformational unbending. We have conducted siRNA knockout experiments that will be reported elsewhere which so far have been inconclusive.

Regulation of leukocyte recruitment by integrin conformational unbending

The current paradigm of leukocyte homing to peripheral sites and lymphoid tissues implies an integration of consecutive chemokine signals while leukocytes roll on endothelium. This integration is believed to cause an increase in the cell adhesion avidity and firm arrest on vascular endothelium (40). A recently published report suggests that the stepwise activation of rolling lymphocytes by chemokine signals is not necessary for the induction of firm arrest for LFA-1 integrin dependent rolling (41). Additionally, it was argued that the extension of the integrin primes for ligand binding and firm adhesion. Our results suggest that due to the short-lived affinity change and long lifetime for the conformational unbending of the integrin, the chemokine signal would increase capture efficiency, and could lead to an increase in the fraction of rolling cells as well as higher tether frequency (Fig. 10*B*). In a real-life situation, leukocytes are exposed to high concentrations of chemokines only on the endothelial cell surface because the constant blood flow "washes away" soluble molecules, or because the chemokines are immobilized on the surface of vascular endothelial cells (42). In this case, integrin activation can be spatially and temporally restricted to the site of cell-to-cell contact (43). However, if the lifetime of the affinity change is short and transient, only conformational unbending will be detected at later times. Such a scenario was described recently by Shamri et al. (41) for LFA-1 and immobilized chemokines.

One of the important results of this report is that rather than being intrinsically related to the affinity change of the binding pocket, the conformational unbending of the integrin molecule is regulated by a different signaling pathway in a different temporal fashion. This may open new directions in the field of regulation of integrin dependent adhesion. Our real-time FRET-based technology for the detection of integrin conformational unbending may promote reevaluation of the existing data. This will provide a better understanding of the complex molecular mechanism that regulates leukocyte recruitment, rolling, and arrest on inflamed endothelium.

Acknowledgments

We thank Eric R. Prossnitz for providing U937 cells and plasmids, and Bruce S. Edwards for providing FCSQuery software.

Disclosures

The authors have no financial conflict of interest.

References

1. Springer, T. A. 1994. Traffic signals for lymphocyte recirculation and leukocyte emigration: the multistep paradigm. *Cell* 76: 301–314.

2. Grabovsky, V., S. Feigelson, C. Chen, D. A. Bleijs, A. Peled, G. Cinamon, F. Baleux, F. Arenzana-Seisdedos, T. Lapidot, Y. van Kooyk, et al. 2000. Subsecond induction of α_4 integrin clustering by immobilized chemokines stimulates leukocyte tethering and rolling on endothelial vascular cell adhesion molecule 1 under flow conditions. *J. Exp. Med.* 192: 495–506.
3. Carman, C. V., and T. A. Springer. 2003. Integrin avidity regulation: are changes in affinity and conformation underemphasized? *Curr. Opin. Cell Biol.* 15: 547–556.
4. Xiong, J. P., T. Stehle, B. Diefenbach, R. Zhang, R. Dunker, D. L. Scott, A. Joachimiak, S. L. Goodman, and M. A. Arnaout. 2001. Crystal structure of the extracellular segment of integrin $\alpha_V\beta_3$. *Science* 294: 339–345.
5. Adair, B. D., J. P. Xiong, C. Maddock, S. L. Goodman, M. A. Arnaout, and M. Yeager. 2005. Three-dimensional EM structure of the ectodomain of integrin $\alpha_V\beta_3$ in a complex with fibronectin. *J. Cell Biol.* 168: 1109–1118.
6. Chigaev, A., T. Buranda, D. C. Dwyer, E. R. Prossnitz, and L. A. Sklar. 2003. FRET detection of cellular α_4 integrin conformational activation. *Biophys. J.* 85: 3951–3962.
7. Chigaev, A., G. J. Zwartz, T. Buranda, B. S. Edwards, E. R. Prossnitz, and L. A. Sklar. 2004. Conformational regulation of $\alpha_4\beta_1$ integrin affinity by reducing agents: "inside-out" signaling is independent of and additive to reduction-regulated integrin activation. *J. Biol. Chem.* 279: 32435–32443.
8. Takagi, J., B. M. Petre, T. Walz, and T. A. Springer. 2002. Global conformational rearrangements in integrin extracellular domains in outside-in and inside-out signaling. *Cell* 110: 599–511.
9. Beglova, N., S. C. Blacklow, J. Takagi, and T. A. Springer. 2002. Cysteine-rich module structure reveals a fulcrum for integrin rearrangement upon activation. *Nat. Struct. Biol.* 9: 282–287.
10. Takagi, J., and T. A. Springer. 2002. Integrin activation and structural rearrangement. *Immunol. Rev.* 186: 141–163.
11. Salas, A., M. Shimaoka, A. N. Kogan, C. Harwood, U. H. von Andrian, and T. A. Springer. 2004. Rolling adhesion through an extended conformation of integrin $\alpha_L\beta_2$ and relation to α_I and β_I-like domain interaction. *Immunity* 20: 393–406.
12. Alon, R., P. D. Kassner, M. W. Carr, E. B. Finger, M. E. Hemler, and T. A. Springer. 1995. The integrin VLA-4 supports tethering and rolling in flow on VCAM-1. *J. Cell Biol.* 128: 1243–1253.
13. Alon, R., and S. Feigelson. 2002. From rolling to arrest on blood vessels: leukocyte tap dancing on endothelial integrin ligands and chemokines at sub-second contacts. *Semin. Immunol.* 14: 93–104.
14. Calzada, M. J., M. V. Alvarez, and J. Gonzalez-Rodriguez. 2002. Agonist-specific structural rearrangements of integrin $\alpha_{IIb}\beta_3$: confirmation of the bent conformation in platelets at rest and after activation. *J. Biol. Chem.* 277: 39899–39908.
15. Shimaoka, M., J. Takagi, and T. A. Springer. 2002. Conformational regulation of integrin structure and function. *Annu. Rev. Biophys. Biomol. Struct.* 31: 485–516.
16. Chigaev, A., A. M. Blenc, J. V. Braaten, N. Kumaraswamy, C. L. Kepley, R. P. Andrews, J. M. Oliver, B. S. Edwards, E. R. Prossnitz, R. S. Larson, and L. A. Sklar. 2001. Real time analysis of the affinity regulation of α_4 integrin: the physiologically activated receptor is intermediate in affinity between resting and Mn^{2+} or antibody activation. *J. Biol. Chem.* 276: 48670–48678.
17. Chigaev, A., G. Zwartz, S. W. Graves, D. C. Dwyer, H. Tsuji, T. D. Foutz, B. S. Edwards, E. R. Prossnitz, R. S. Larson, and L. A. Sklar. 2003. $\alpha_4\beta_1$ integrin affinity changes govern cell adhesion. *J. Biol. Chem.* 278: 38174–38182.
18. Hernandez-Hansen, V., A. J. Smith, Z. Surviladze, A. Chigaev, T. Mazel, J. Kalesnikoff, C. A. Lowell, G. Krystal, L. A. Sklar, B. S. Wilson, and J. M. Oliver. 2004. Dysregulated FcεRI signaling and altered Fyn and SHIP activities in Lyn-deficient mast cells. *J. Immunol.* 173: 100–112.
19. Zwartz, G. J., A. Chigaev, D. C. Dwyer, T. D. Foutz, B. S. Edwards, and L. A. Sklar. 2004. Real-time analysis of very late antigen-4 affinity modulation by shear. *J. Biol. Chem.* 279: 38277–38286.
20. Kew, R. R., T. Peng, S. J. DiMartino, D. Madhavan, S. J. Weinman, D. Cheng, and E. R. Prossnitz. 1997. Undifferentiated U937 cells transfected with chemoattractant receptors: a model system to investigate chemotactic mechanisms and receptor structure/function relationships. *J. Leukocyte Biol.* 61: 329–337.
21. Osborn, L., C. Hession, R. Tizard, C. Vassallo, S. Luhowskyj, G. Chi-Rosso, and R. Lobb. 1989. Direct expression cloning of vascular cell adhesion molecule 1, a cytokine-induced endothelial protein that binds to lymphocytes. *Cell* 59: 1203–1211.
22. Hsu, M. H., S. C. Chiang, R. D. Ye, and E. R. Prossnitz. 1997. Phosphorylation of the *N*-formyl peptide receptor is required for receptor internalization but not chemotaxis. *J. Biol. Chem.* 272: 29426–29429.
23. Prossnitz, E. R. 1997. Desensitization of *N*-formylpeptide receptor-mediated activation is dependent upon receptor phosphorylation. *J. Biol. Chem.* 272: 15213–15219.
24. Parker, P. J., and J. Murray-Rust. 2004. PKC at a glance. *J. Cell Sci.* 117: 131–132.
25. Jin, J., V. R. Dasari, F. D. Sistare, and S. P. Kunapuli. 1998. Distribution of P2Y receptor subtypes on haematopoietic cells. *Br. J. Pharmacol.* 123: 789–794.
26. Neelamegham, S., A. D. Taylor, J. D. Hellums, M. Dembo, C. W. Smith, and S. I. Simon. 1997. Modeling the reversible kinetics of neutrophil aggregation under hydrodynamic shear. *Biophys. J.* 72: 1527–1540.
27. Zwartz, G., A. Chigaev, T. Foutz, R. S. Larson, R. Posner, and L. A. Sklar. 2004. Relationship between molecular and cellular dissociation rates for VLA-4/VCAM-1 interaction in the absence of shear stress. *Biophys. J.* 86: 1243–1252.
28. Edwards, B. S., F. W. Kuckuck, E. R. Prossnitz, A. Okun, J. T. Ransom, and L. A. Sklar. 2001. Plug flow cytometry extends analytical capabilities in cell adhesion and receptor pharmacology. *Cytometry* 43: 211–216.
29. Chen, S., and T. A. Springer. 1999. An automatic braking system that stabilizes leukocyte rolling by an increase in selectin bond number with shear. *J. Cell Biol.* 144: 185–200.
30. Chen, L. L., A. Whitty, R. R. Lobb, S. P. Adams, and R. B. Pepinsky. 1999. Multiple activation states of integrin $\alpha_4\beta_1$ detected through their different affinities for a small molecule ligand. *J. Biol. Chem.* 274: 13167–13175.
31. Feigelson, S. W., V. Grabovsky, E. Winter, L. L. Chen, R. B. Pepinsky, T. Yednock, D. Yablonski, R. Lobb, and R. Alon. 2001. The Src kinase $p56^{lck}$ up-regulates VLA-4 integrin affinity: implications for rapid spontaneous and chemokine-triggered T cell adhesion to VCAM-1 and fibronectin. *J. Biol. Chem.* 276: 13891–13901.
32. Kucik, D. F., M. L. Dustin, J. M. Miller, and E. J. Brown. 1996. Adhesion-activating phorbol ester increases the mobility of leukocyte integrin LFA-1 in cultured lymphocytes. *J. Clin. Invest.* 97: 2139–2144.
33. Rose, D. M., P. M. Cardarelli, R. R. Cobb, and M. H. Ginsberg. 2000. Soluble VCAM-1 binding to α_4 integrins is cell-type specific and activation dependent and is disrupted during apoptosis in T cells. *Blood* 95: 602–609.
34. Jakubowski, A., M. D. Rosa, S. Bixler, R. Lobb, and L. C. Burkly. 1995. Vascular cell adhesion molecule (VCAM)-Ig fusion protein defines distinct affinity states of the very late antigen-4 (VLA-4) receptor. *Cell Adhes. Commun.* 3: 131–142.
35. Hynes, R. O. 2002. Integrins: bidirectional, allosteric signaling machines. *Cell* 110: 673–687.
36. Xiong, J. P., T. Stehle, S. L. Goodman, and M. A. Arnaout. 2003. New insights into the structural basis of integrin activation. *Blood* 102: 1155–1159.
37. Disatnik, M. H., and T. A. Rando. 1999. Integrin-mediated muscle cell spreading: the role of protein kinase c in outside-in and inside-out signaling and evidence of integrin cross-talk. *J. Biol. Chem.* 274: 32486–32492.
38. von Andrian, U. H. 2001. PKC-β_I: the whole ignition system or just a sparkplug for T cell migration? *Nat. Immunol.* 2: 477–478.
39. Bleasdale, J. E., N. R. Thakur, R. S. Gremban, G. L. Bundy, F. A. Fitzpatrick, R. J. Smith, and S. Bunting. 1990. Selective inhibition of receptor-coupled phospholipase C-dependent processes in human platelets and polymorphonuclear neutrophils. *J. Pharmacol. Exp. Ther.* 255: 756–768.
40. Jung, U., K. E. Norman, K. Scharffetter-Kochanek, A. L. Beaudet, and K. Ley. 1998. Transit time of leukocytes rolling through venules controls cytokine-induced inflammatory cell recruitment in vivo. *J. Clin. Invest.* 102: 1526–1533.
41. Shamri, R., V. Grabovsky, J. M. Gauguet, S. Feigelson, E. Manevich, W. Kolanus, M. K. Robinson, D. E. Staunton, U. H. von Andrian, and R. Alon. 2005. Lymphocyte arrest requires instantaneous induction of an extended LFA-1 conformation mediated by endothelium-bound chemokines. *Nat. Immunol.* 6: 497–506.
42. Johnston, B., and E. C. Butcher. 2002. Chemokines in rapid leukocyte adhesion triggering and migration. *Semin. Immunol.* 14: 83–92.
43. Laudanna, C. 2005. Integrin activation under flow: a local affair. *Nat. Immunol.* 6: 429–430.